J Therm Spray Tech (2021) 30:1557–1565
https://doi.org/10.1007/s11666-021-01234-7

PEER REVIEWED

Corrosion Behavior of Arc-Sprayed Pore-Sealed Zn and Al Coatings in Seawater Containing Sulfate-Reducing Bacteria (SRB)

Lei Qiao[1] · Yuping Wu[1,2] · Jizhou Duan[3] · Wenwen Gao[1] · Sheng Hong[1]

Submitted: 4 December 2020 / in revised form: 4 May 2021 / Accepted: 21 June 2021 / Published online: 7 July 2021

Abstract In this article, zinc and aluminum coatings were deposited on plain carbon structural steel (Q235) substrates by electric arc spraying. The coatings were then pore-sealed with a silicone resin to enhance their corrosion performance. The latter was tested in seawater containing sulfate-reducing bacteria by open circuit potential, potentiodynamic polarization and electrochemical impedance spectroscopy. The tests showed that the pore-sealed Al coating had a superior corrosion resistance to the pore-sealed Zn coating in all the corrosion tests. The corrosion rates of the pore-sealed Zn coating first increased as the oxide film was easily destroyed. Then, they decreased as the corrosion products delayed the diffusion of the corrosive medium. On the other hand, the corrosion rates of the pore-sealed Al coating consistently decreased, most likely because of the protective effect of the dense Al_2O_3 film formed at the early stage of immersion and biological film formed by SRB at the later stage of immersion.

Keywords corrosion · electric arc spraying · pore-sealed Al coating · pore-sealed Zn coating · sulfate-reducing bacteria

✉ Yuping Wu
wuyuping@hhu.edu.cn

[1] College of Mechanics and Materials, Hohai University, 8 Focheng West Road, Nanjing 211100, People's Republic of China

[2] Jiangsu Key Laboratory of Advanced Structural Materials and Application Technology, 1 Hongjing Avenue, Nanjing 211100, People's Republic of China

[3] Institute of Oceanology, Chinese Academy of Sciences, 7 Nanhai Road, Qingdao 266071, People's Republic of China

Introduction

The corrosion problem of carbon steels is a great handicap for usage of these materials in marine environments (Ref 1-3). There are many factors that can induce the corrosive damage of simple steel components in the marine environment, including the chloride ion-induced corrosion and microbial influenced corrosion (MIC) (Ref 4). Preparing coatings on carbon steels is a versatile method to improve their chloride ion-induced corrosion and microbial influenced corrosion performance (Ref 5, 6).

Up to now, a great number of methods have been used to produce coatings on steel substrates used in seawater, including vapor deposition method (Ref 7), ion beam assisted deposition method (Ref 8), sputtering method (Ref 9), etc. However, these methods usually exhibit low deposition efficiency and cannot prepare thick coatings, which limit their application in prolonging the service life of steel components. Thermal spraying is one of the best technologies to deposit thick coatings with several hundreds of micrometers (Ref 10-13). Among various thermal spraying technologies, electric arc spraying technology has been widely used in metal protection because of its low cost, high efficiency, easy operation and excellent performance (Ref 14, 15). Nevertheless, the arc-sprayed coatings usually have certain porosity, resulting in permeation of corrosive medium much easier and thus degrading their corrosion performance. Hence, the pore-sealing treatment is necessary and significant for the electric arc-sprayed coatings before their application in seawater (Ref 16, 17).

To have good chloride ion-induced corrosion and microbial influenced corrosion simultaneously, the early coatings used for preventing the substrate from biological corrosion are usually not environmentally friendly, such as the coatings containing Sn, Cu, Pb or Hg (Ref 18). Recently,

some advanced coatings such as bionic antifouling coatings or low surface antifouling coatings were developed. These coatings usually have superior biological corrosion resistance and do no harm to the environment. However, the preparation difficulty and cost of these coatings are both high (Ref 19). Hence, as typical anti-corrosion materials, environmentally friendly Zn and Al coatings have been widely used in the marine environment and related research concerning their corrosion behavior and mechanism has been conducted.

Liu et al. (Ref 20) studied the corrosion resistance of zinc-coated steel (ZCS) in seawater, and they found that the corrosion rate of ZCS elevated with the increase in immersion time. Besides, they also proved that the porous and loose corrosion products of the ZCS mainly consisted of ZnO, $Zn_5(OH)_8Cl_2$, and $Zn_5(OH)_6(CO_3)_2$. Open circuit potential and zero-resistance ammetry techniques were used by Stoulil et al. (Ref 21) to monitor the electrochemical corrosion behavior of aluminum alloys in various environments, including seawater, artificial rain, and the atmosphere. The experiments showed that the aluminum alloys had promising corrosion performance and electrochemical behavior characteristics.

Though the chloride ion-induced corrosion performances of zinc coating and aluminum coating have been studied in diverse environments (including atmosphere, acids, chlorides, etc.), the research about the microbial influenced corrosion performance of these coatings still lacks (Ref 22, 23). As an anaerobic microbe widely exists in oxygen-deprived marine environments, sulfate-reducing bacteria (SRB) is taken as a main reason to induce the microbial influenced corrosion of metals in the sea. In anaerobic conditions, the SRB will grow into bio-community and form metabolites such as S^{2-} and H_2S. These metabolites can reduce the metals to sulfides and cause the corrosion of the metals (Ref 24, 25). Hence, the electrochemical behavior and relevant mechanism of electric arc-sprayed Zn coating and Al coating in seawater containing SRB and the role of SRB in corrosion process is worth researching.

In the present work, the open circuit potential (OCP), potentiodynamic polarization (PDP) and electrochemical impedance spectroscopy (EIS) techniques were applied to analyze the corrosion behavior of pore-sealed Zn coating and Al coating deposited by arc spray technology in SRB seawater. The corrosion mechanism of pore-sealed Zn coating and Al coating was also discussed by using the scanning electron microscopy (SEM) and energy dispersive spectroscopy (EDS).

Experimental

Fabrication of the Coatings

Pure Zn (99.9 wt.%) and Al (99.9 wt.%) wires with diameter of 3 mm were used as the raw material. The Q235 carbon steel was selected as substrate. Table 1 lists the nominal composition of the steel. The substrate was previously machined, rinsed in alcohol and sandblasted with corundum powder prior to spraying by a CD-500 electric arc spray system. The spraying parameters of both pure Zn and Al wires were controlled as 200 mm for the spray distance, 32 V for the spray voltage, 120 A for the spray current and 0.65 MPa for the air pressure.

After spraying, all the samples were pore-sealed with silicone resin to promote the corrosion performance. In this work, a silicone resin with technical index shown in Table 2 was used as sealant. Prior to sealing, the coatings were ultrasonically cleaned and dried at 60 °C. The cleaned surface of the coatings was then coated with appropriate amount of sealing agent with a brush, and dried at 115 °C for 30 min. Finally, the redundant silicone resin was polished by abrasive paper.

SRB Cultivation and Experimental Medium

The SRB strains applied in this experiment were derived from sludge in Kiaochow Bay, Shandong. Afterward, modified Postgate's culture medium was used to enrich and culture the SRB strains. The aforementioned medium consisted of 0.06 g $MgSO_4 \cdot 7H_2O$, 0.06 g $CaCl_2 \cdot 6H_2O$, 0.3 g Na-citrate, 0.5 g KH_2PO_4, 1.0 g NH_4Cl, 1.0 g yeast cream and 6 mL 70% sodium lactate per liter seawater. The medium should be sterilized by high-pressure steam at 121 °C for 20 min, then 0.004 g/L $Fe(NH_4)_2(SO_4)_2 \cdot 7H_2O$ was also added to the medium. Finally, the seawater was added with 5 vol.% pure bacterium solution to form the experimental medium.

Experimental Methods

The electrochemical system comprised a 1260A frequency response analyzer (Solartron) and a 1287 potentiostat (Solartron) was applied to measure the corrosion performance of pore-sealed Zn coating and Al coating in seawater containing SRB. Before the test, the samples were encapsulated in non-conducting colophony and only an end-surface with a square area of about 1 cm^2 was exposed to the medium. A classic three electrode cell was used to conduct the electrochemical

Table 1 The chemical composition of Q235 steel

Elements	C	Si	Mn	P	S	Fe
Composition (wt.%)	0.14-0.22	≤ 0.35	≤ 0.14	≤ 0.045	≤ 0.05	Bal.

Table 2 Technical index of silicon resin

pH	Viscosity, Pa s; 25 ± 1 °C	Density, g cm^{-3}; 25 ± 1 °C	Adhesive capacity	Dielectric strength, kV mm^{-1}
6-7	9.7-14.0	0.87-0.95	1	30-50

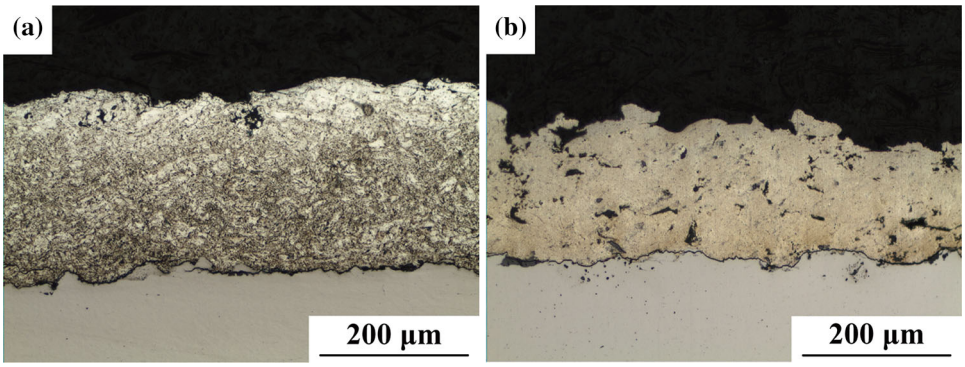

Fig. 1 Optical cross-sectional micrographs of as-sprayed Zn coating (a) and Al coating (b)

tests, with a saturated calomel system as reference electrode, a 10 × 20 mm Ruthenium-Titanium plate as auxiliary electrode, and the specimen as working electrode. These electrodes should be sterilized with an ultraviolet lamp for 30 min before conducting the experiment. In the experimental process, the corrosive medium should be replaced every 24 h to ensure the consistency of corrosive environments. The electrochemical impedance spectroscopy (EIS) test was measured at open circuit potential (OCP) with a sine wave potential perturbation of 10 mV in a frequency fluctuating from 10 mHz to 100 kHz. The potentiodynamic polarization test ranged from − 0.4 to 0.4 V_{SCE} relative to the OCP at a constant rate of 0.5 mV/s.

The surface morphologies and elements of the pore-sealed Zn coating and Al coating after electrochemical tests were observed by scanning electron microscopy (SEM) and analyzed by energy dispersive spectroscopy (EDS). Before observation, the samples should be immersed in testing medium for 15 days, and then washed by sterile seawater three times. After that, the samples should be immersed in 5 vol.% pentanediol solution for 30 min to set the bacterium on their surfaces, finally dehydrated with different gradient of ethanol (50%, 70%, and 100%) in sequence and dried in a vacuum environment.

Results and Discussions

Coating Characterization

Figure 1 shows the typical cross-sectional morphologies of the as-sprayed Zn coating and Al coating. Both coatings exhibit similar thickness. The thickness of the Zn coating is about 230 μm, while the thickness of the Al coating is about 200 μm. As shown in Fig. 1(a), the Zn coating had distinct layered structure, and some obvious pores or micro-cracks can be observed between the layers. This is because during the process of arc spraying, most of the particles were deposited on the substrate or the former layer in a melted or half-melted state. These particles deformed under the impact effect and then formed splats. The gas porosity phenomenon and loose-packed layer structure resulted in the pores and micro-cracks between the splats. In addition, the volume shrinkage of droplets led to the pores and micro-cracks within the splats (Ref 26). However, the lamellar structure of the Al coating is not obvious, which could be ascribed to the high melting degree of the Al particles during the spraying process. The inherent characteristics of the arc-sprayed coatings, including pores and micro-cracks, could also be found in the Al coating (Ref 27). Based on the grayscale

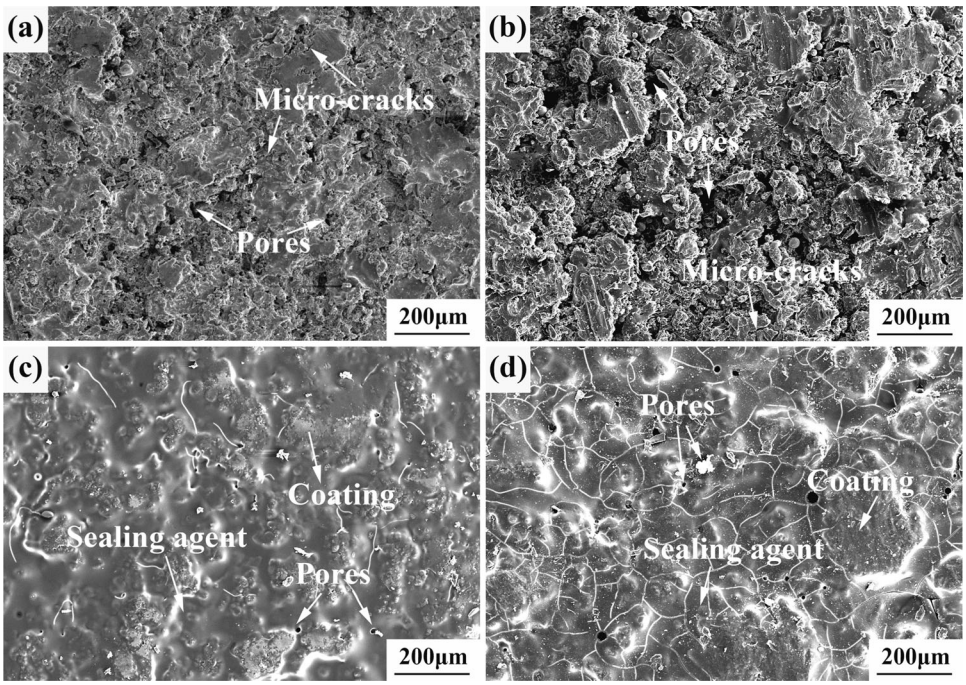

Fig. 2 SEM surface micrographs of Zn coatings (a, c) and Al coatings (b, d): (a), (b) as-sprayed; (c), (d) pore-sealed

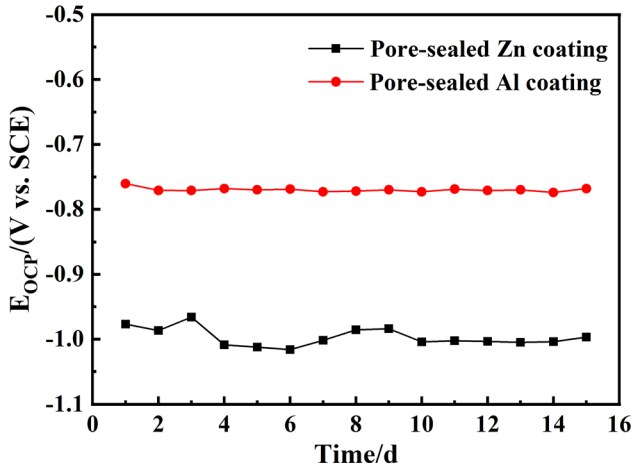

Fig. 3 Open circuit potential-time curves of pore-sealed Zn coating and Al coating in SRB seawater

threshold method (Ref 28), the porosity of as-sprayed Zn coating and Al coating is calculated to be 3.1% and 7.6%, respectively.

The typical surface morphologies of the as-sprayed and pore-sealed Zn and Al coatings are illustrated in Fig. 2. It can be clearly found that some pores and micro-cracks are distributed on the surface of Zn (Fig. 2a) and Al (Fig. 2b) coatings. It is generally accepted that the pores and micro-cracks in thermal sprayed coatings are extremely detrimental to their performance (Ref 29). Hence, the pore-sealing treatment of the as-sprayed coatings is necessary for their practical applications. The commercially available silicone used in this study exhibited good sealing property because of its excellent liquidity and penetrability. After pore-sealing treatment, the surface morphologies of pore-sealed Zn and Al coatings can be seen in Fig. 2(c), (d), respectively. It could be obviously observed that the pores and micro-cracks were effectively blocked, thus the pore-sealed coatings exhibited less pores and micro-cracks compared to the as-sprayed coatings.

Open circuit Potential

Figure 3 shows the open circuit potential (OCP) of pore-sealed Zn coating and Al coating in SRB seawater for different immersion times. In the first 6 days, the OCP of the pore-sealed Zn coating fluctuated downward from − 976 to − 1025 mV. This is because with the diffusion of corrosion medium (Cl^-, S^{2-}, etc.), the ZnO film on pore-sealed Zn coating would be dissolved, and the partial failure of oxide film directly resulted in the decrease in OCP (Ref 30). From 6 to 9 days, the OCP had a slow growth from − 1025 to − 980 mV. This phenomenon could be ascribed to the formation and aggregation of corrosion products and the accumulation of SRB, which would reduce the porosity in the coatings and delay the diffusion of corrosive liquid (Ref 31, 32). After 9 days, the OCP kept at a basically stable value of − 1002 mV, which manifested the electrochemical corrosion kinetics of the specimen reached relative stability. For the pore-sealed Al coating, the OCP maintained at a stable value of about − 772 mV during the whole testing process. This is because of the protective effect of dense alumina film formed on the surface of the coating (Ref 15, 33).

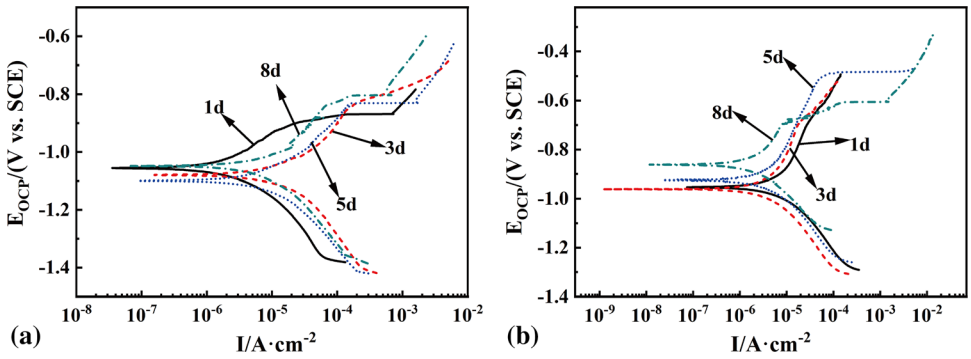

Fig. 4 Polarization curves of pore-sealed Zn coatings (a) and Al coatings (b) in SRB seawater

Table 3 Corrosion potentials (E_{corr}) and corrosion current densities (i_{corr}) of pore-sealed Zn coatings and Al coatings

Time/d	E_{corr}/V		i_{corr}/(A cm^{-2})	
	Zn	Al	Zn	Al
1	− 1.054	− 0.953	3.754×10^{-6}	3.093×10^{-6}
3	− 1.076	− 0.961	6.123×10^{-6}	2.247×10^{-6}
5	− 1.097	− 0.925	4.889×10^{-6}	2.029×10^{-6}
8	− 1.049	− 0.882	4.134×10^{-6}	1.191×10^{-6}

Meanwhile, it could be found that the OCP of the pore-sealed Al coating is consistently higher than that of the pore-sealed Zn coating throughout this experiment, which signified that in SRB seawater the pore-sealed Al coating showed superior corrosion resistance to the pore-sealed Zn coating.

Potentiodynamic Polarization Analyses

Figure 4 shows the Tafel polarization curves of pore-sealed Zn coatings (a) and Al coatings (b) in seawater containing SRB for different immersion times. The obtained corrosion potential (E_{corr}) and current density (i_{corr}) for each curve were tabulated in Table 3.

As presented in Table 3, it could be found that the i_{corr} of the pore-sealed Zn coatings increased from 3.754×10^{-6} to 6.123×10^{-6} A cm^{-2} at first, and then decreased to 4.134×10^{-6} A cm^{-2} with the increase of immersion time. This is mainly because a large number of metabolites with high causticity were produced in the early immersion period. These metabolites and chloride ions kept attacking the coatings and increasing the corrosion rate of the coatings gradually. Afterward, the corrosion products formed on the surface and blocked the pores or micro-cracks in the coatings, which would protect the coatings from subsequent damage and decrease their corrosion rates (Ref 2). However, the i_{corr} of the pore-sealed Al coatings kept decreasing from 3.093×10^{-6} to 1.191×10^{-6} A cm^{-2} throughout the test, this could be due to the outstanding protective effect of dense alumina film. As corrosion time goes on, the accumulation of SRB further prevented the pore-sealed Al coatings from being destroyed (Ref 34, 35).

Throughout the course of the experiment, the pore-sealed Al coating presented higher corrosion potential along with lower corrosion current density than the pore-sealed Zn coating, suggesting that the pore-sealed Al coating showed better corrosion performance than the pore-sealed Zn coating in seawater with SRB. The Tafel polarization results are in good agreement with the above OCP results.

Electrochemical Impedance Spectra

To further elucidate the corrosion behavior of pore-sealed Zn coating and Al coating in seawater containing SRB, EIS measurement was performed, and the results were illustrated in Fig. 5. As shown in Fig. 5(a), the Nyquist plots of pore-sealed Zn coatings all showed two capacitive arcs, i.e., a capacitive arc at high frequency which is corresponding to the capacitance and resistance of coating, and a capacitive arc at low frequency which is corresponding to the capacitance of double electric layer and the resistance of electrochemical reaction at solution/coating interface (Ref 36). For pore-sealed Zn coating, it can be found that the arc diameter at low frequency reduced greatly after immersion for 2 days, which is due to destruction of oxide films formed on the coatings. From 3 to 15 days, the arc diameters of the coatings fluctuated slightly. Hence, as the immersion time prolongs, the corrosion resistance of the pore-sealed Zn coatings decreased first and then remained relatively stable. Figure 5(b) shows the Nyquist plots of pore-sealed Al coating in SRB seawater. The arc diameters of impedance plots remained stable from 1 to 5 days, and then increased from 5 to 15 days. The results revealed that the corrosion rates of pore-sealed Al coatings kept relatively stable during the early period, and then decreased.

To better explain the corrosion behavior of these coatings, an equivalent circuit (as shown in Fig. 6) was applied for the simulation of EIS data. The $R_s(Q_c(R_c(Q_{dl}R_{ct})))$ circuit is commonly used for metal/oxide layer/electrolyte system (Ref 37), where R_s, R_c, R_{ct}, Q_c, and Q_{dl} represent the

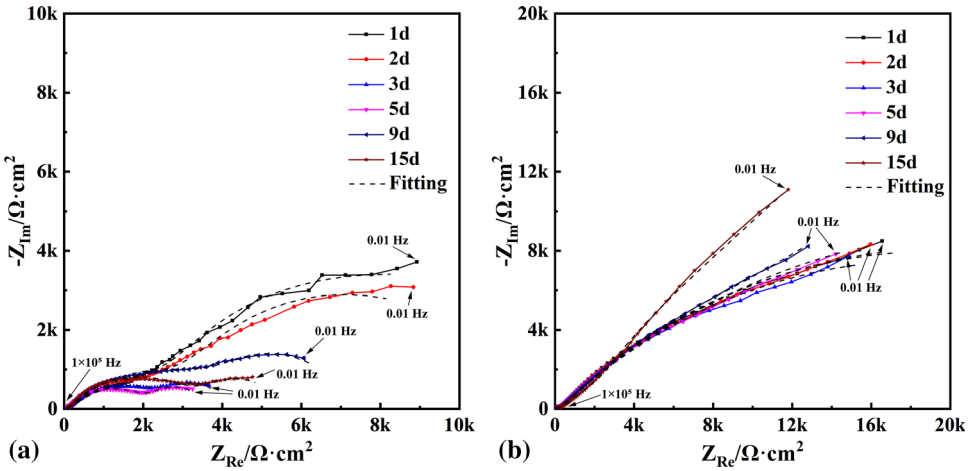

Fig. 5 Nyquist plots of pore-sealed Zn coatings (a) and Al coatings (b) in SRB seawater

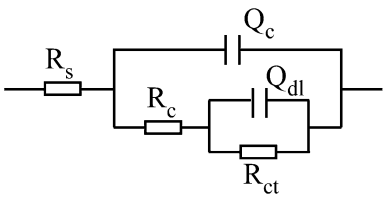

Fig. 6 The equivalent circuit used for EIS analysis in this study

resistance of solution, the resistance of the coating, the charge transfer resistance of the corrosion reaction, the capacitance of the coating, and the capacitance of the double layer or oxide film, respectively. A ZSimpwin software was applied to fit the EIS plots to obtain the equivalent circuit parameters, which were listed in Tables 4 and 5.

It could be found from Table 4 that the R_{ct} values of the pore-sealed Zn coatings were relatively large at the initial stage (1-2 days). This is because a protective film composed of oxide film and silicone resin retarded the diffusion of corrosive liquid effectively. After 2 days of immersion, the R_{ct} values decreased rapidly, which could be attributed to the dissolution of ZnO film and the penetration of corrosive medium through these active zones (Ref 38). As corrosion time increased from 5 to 15 days, the R_{ct} values increased slowly, which is mainly due to the combined effect of SRB and their metabolites. As corrosion time further increased, a large number of metabolites would be produced and then reacted with the dissolved Zn^{2+} to form corrosion products, such as ZnS. These corrosion products adhered to the coating or plugged the pores in the coating, thus retarding further corrosion (Ref 39). For the pore-sealed Al coatings, it can be seen from Table 5 that the R_{ct} values showed a slight fluctuating rise during the first 5 days. Similar to the pore-sealed Zn coatings, the main reason could be due to the protective film which consisted of silicone resin and oxidation film. However, after immersion for 5 days, the R_{ct} values of the pore-sealed Al coatings increased rapidly. This is because with the prolongation of the immersion time, the SRB proliferated continuously and then deposited on the dense Al_2O_3 film to form biofilms. The deposited biofilms can further prevent the coatings from being attacked by the corrosive medium, and thus improve the corrosion performance of the coatings (Ref 40, 41).

Besides, it is obvious that the R_{ct} values of the pore-sealed Al coatings were much larger than that of the pore-sealed Zn coatings. This could be ascribed to the different oxidation films formed on the coatings. Considering the oxide film of the pore-sealed Al coatings is quite dense and hard to be dissolved in corrosive liquid, the film can prevent the coatings from being corroded effectively. However, the oxide film of the pore-sealed Zn coating is easy to destroy in corrosive medium (Ref 42). In consequence, the pore-sealed Al coatings exhibited better corrosion performance than the pore-sealed Zn coatings in the SRB seawater.

Surface Morphologies After Corrosion

After soaking for 15 days, the SEM images and EDS analyses of the pore-sealed Al coating and Zn coating in seawater containing SRB were shown in Fig. 7. It can be seen from Fig. 7(a) that some corrosion products and irregular particles were distributed on the eroded surface of pore-sealed Zn coating. These particles were supposed to be the coatings peeled off under the joint effect of corrosive medium and SRB. While in Fig. 7(b), a covering film with fewer corrosion products could be found on the surface of pore-sealed Al coating. The covering film on the surface of pore-sealed Al coating was relatively homogeneous, but the covering film on the surface of pore-sealed Zn coating was looser. In order to better understand the corrosion mechanism, EDS measurement was conducted. The EDS results showed that both pore-sealed Zn coating and Al coating contained C, O, P, S, and Si. It can be observed that the S content on the surface of pore-sealed Al coating is lower than that of pore-sealed Zn

Table 4 Electrochemical parameters of pore-sealed Zn coatings in SRB seawater acquired from EIS plots

Time (d)	R_s, Ω cm^{-2}	Q_c, μF cm^{-2}	n_1	R_c, kΩ cm^{-2}	Q_{dl}, μF cm^{-2}	n_2	R_{ct}, kΩ cm^{-2}
1	37.51	84.31	0.4422	2.552	273.5	0.7151	12.15
2	28.80	40.28	0.5354	2.025	313.1	0.6129	10.85
3	38.83	40.06	0.4924	1.762	248.3	0.6113	1.739
5	29.80	45.55	0.5743	1.906	120.6	0.5851	2.341
9	29.96	60.65	0.5596	2.025	356.0	0.5813	2.995
15	25.40	59.58	0.5723	2.182	328.9	0.54	3.043

Table 5 Electrochemical parameters of pore-sealed Al coatings in SRB seawater acquired from EIS plots

Time, d	R_s, Ω cm^{-2}	Q_c, μF cm^{-2}	n_1	R_c, kΩ cm^{-2}	Q_{dl}, μF cm^{-2}	n_2	R_{ct}, kΩ cm^{-2}
1	34.2	59.52	0.518	2.949	319.8	0.5591	37.74
2	28.42	71.40	0.4939	3.324	249.5	0.5882	37.01
3	25.38	67.17	0.4928	3.212	265.5	0.5653	38.58
5	20.25	54.13	0.4313	3.342	186.3	0.5153	40.95
9	31.31	51.56	0.4239	3.704	66.10	0.4765	56.78
15	34.46	50.83	0.4369	3.823	64.30	0.4481	70.42

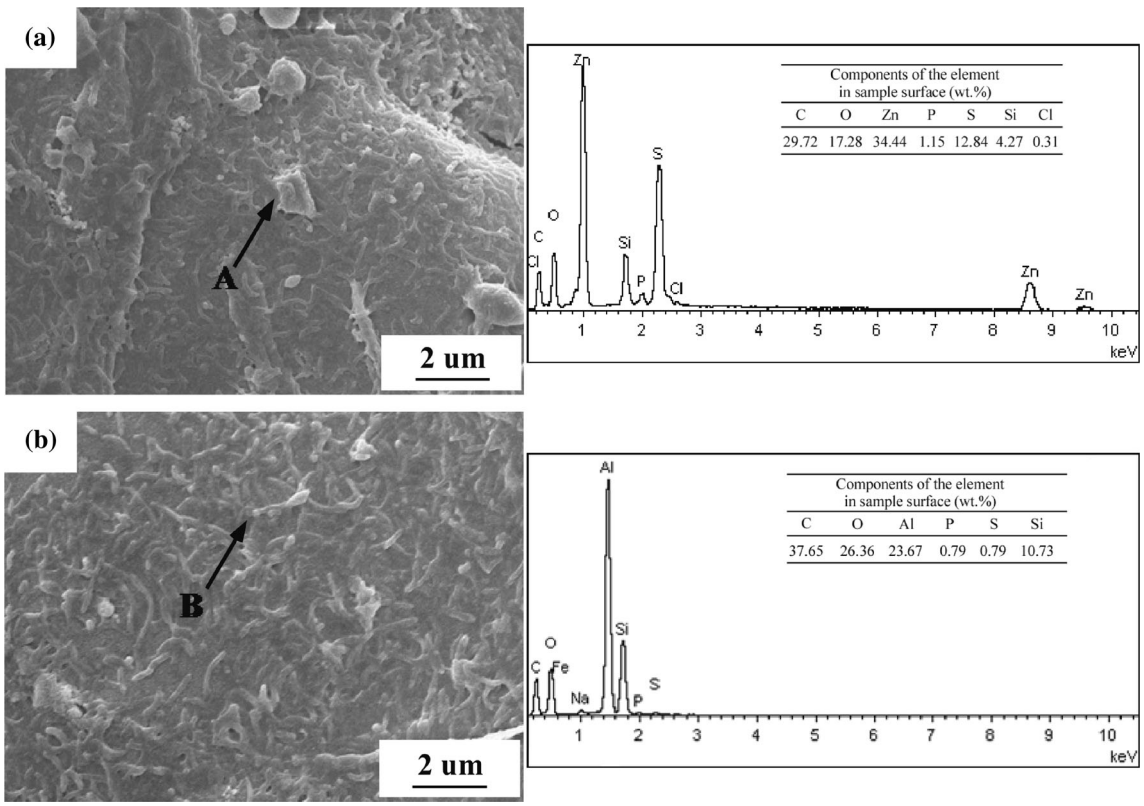

Fig. 7 SEM images and EDS analyses of pore-sealed Zn coating (a) and Al coating (b) after corrosion in SRB seawater

coating. Because the dense Al_2O_3 film is hard to be corroded in the corrosive medium, few aluminums can react with SRB metabolites (such as H_2S, S^{2-}, and other S-containing metabolites) to produce S-containing corrosion products (Ref 43). This result can also prove that the pore-sealed Al coating exhibited better corrosion performance than the pore-sealed Zn coating in SRB seawater.

Conclusions

(1) Both arc-sprayed Zn coating and Al coating exhibited many pores and micro-cracks. After pore-sealing treatment, the pores and micro-cracks of the coatings were effectively blocked.

(2) The corrosion rate of pore-sealed Zn coating increased first and then decreased, while the corrosion rate of pore-sealed Al coating kept decreasing. This is because the oxide film of pore-sealed Zn coatings is easier to destroy at the early stage of the immersion process, but the dense oxide film of pore-sealed Al coating can play a protective function from the beginning of immersion. At later stage of immersion, the corrosion products and the biological film formed on the surface of pore-sealed Zn coating and pore-sealed Al coating can prevent the coatings from being corroded.

(3) In seawater with SRB, the pore-sealed Al coating exhibited better corrosion performance than the pore-sealed Zn coating. For pore-sealed Zn coating, the protective effect is mainly due to the sealing effect of the corrosion products. For pore-sealed Al coating, the protective effect depends on the dense Al_2O_3 film and the biological film which can prevent the invasion of corrosive medium.

Acknowledgments The research was supported by the National Natural Science Foundation of China (Grant Nos. 51579087, 51975183 and 51979083), the Natural Science Foundation of Jiangsu Province, China (Grant No. BK20201316) and the Opening Project of Jiangsu Key Laboratory of Advanced Structural Materials and Application Technology (Grant No. ASMA201902).

References

1. A.A.M.M. Singh, P.A. Franco and J.S. Binoj, Enhancement of Corrosion Resistance on Plasma Spray Coated Mild Steel Substrate Exposed to Marine Environment, *Mater. Today*, 2019, **15**, p 84–89.
2. S.A. Galedari, A. Mahdavi, F. Azarmi, Y. Huang and A. McDonald, A Comprehensive revIew of Corrosion Resistance of Thermally-Sprayed and Thermally-Diffused Protective Coatings on Steel Structures, *J. Therm. Spray Techn.*, 2019, **28**(4), p 645–677.
3. O.S.I. Fayomi, A.P.I. Popoola, L.R. Kanyane and T. Monyai, Development of Reinforced In-situ Anti-Corrosion and Wear Zn-TiO_2/$ZnTiB_2$ Coatings on Mild Steel, *Results Phys.*, 2017, **7**, p 644–650.
4. H.B. Li, E.Z. Zhou, Y.B. Ren, D.W. Zhang, D.K. Xu, C.G. Yang, H. Feng, Z.H. Jiang, X.G. Li, T.Y. Gu and K. Yang, Investigation of Microbiologically Influenced Corrosion of High Nitrogen Nickel-Free Stainless Steel by Pseudomonas Aeruginosa, *Corros. Sci.*, 2016, **111**, p 811–821.
5. Y.W. Ye, H. Chen, Y.J. Zou, Y. Ye and H.C. Zhao, Corrosion Protective Mechanism of Smart Graphene-Based Self-healing Coating on Carbon Steel, *Corros. Sci.*, 2020, **174**, p 108825.
6. P.A. Rasheed, K.A. Jabbar, H.R. Mackey and K.A. Mahmoud, Recent Advancements of Nanomaterials as Coatings and Biocides for the Inhibition of Sulfate Reducing Bacteria Induced Corrosion, *Curr. Opin. Chem. Eng.*, 2019, **25**, p 35–42.
7. S. Sabooni, M. Ahmadi, E. Galinmoghaddam, R.J. Westerwaal, C. Boelsma, E. Zoestbergen, G.M. Song and Y.T. Pei, Fundamentals of the Adhesion of Physical Vapor Deposited ZnMg-Zn Bilayer Coatings to Steel Substrates, *Mater. Des.*, 2020, **190**, p 108560.
8. S.W. Fu, H.J. Chen, H.T. Wu, K.T. Hung and C.F. Shih, Electrical and Optical Properties of Al: ZnO Films Prepared by Ion-Beam Assisted Sputtering, *Ceram. Int.*, 2016, **42**(2), p 2626–2633.
9. N. Nedfors, S. Mráz, J. Palisaitis, P.O.Å. Persson, H. Lind, S. Kolozsvari, J.M. Schneider and J. Rosen, Influence of the Al Concentration in Ti-Al-B Coatings on Microstructure and Mechanical Properties using Combinatorial Sputtering from a Segmented TiB_2/AlB_2 Target, *Surf. Coat. Tech.*, 2019, **364**, p 89–98.
10. P.R.C.A. Junior and A.G.M. Pukasiewicz, Evaluation of Microstructure, Mechanical and Tribological Properties of a Babbitt Alloy Deposited by Arc and Flame Spray Processes, *Tribol. Int.*, 2019, **131**, p 148–157.
11. G. Bolelli, M. Bursi, L. Lusvarghi, T. Manfredini, V. Matikainen, R. Rigon, P. Sassatelli and P. Vuoristo, Tribology of FeVCrC Coatings Deposited by HVOF and HVAF Thermal Spray Processes, *Wear*, 2018, **394**, p 113–133.
12. G. Bolelli, L.M. Berger, T. Börner, H. Koivuluoto, V. Matikainen, L. Lusvarghi, C. Lyphout, N. Markocsan, P. Nylén, P. Sassatelli, R. Trache and P. Vuoristo, Sliding and Abrasive Wear Behaviour of HVOF-and HVAF-Sprayed Cr_3C_2-NiCr Hardmetal Coatings, *Wear*, 2016, **358**, p 32–50.
13. W. Deng, Y.L. An, G.L. Hou, S.J. Li, H.D. Zhou and J.M. Chen, Effect of Substrate Preheating Treatment on the Microstructure and Ultrasonic Cavitation Erosion Behavior of Plasma-Sprayed YSZ Coatings, *Ultrason. Sonochem.*, 2018, **46**, p 1–9.
14. K. Hartz-Behrend, J. Schaup, J. Zierhut and J. Schein, Controlling the Twin Wire Arc Spray Process Using Artificial Neural Networks (ANN), *J. Therm. Spray Techn.*, 2016, **25**(1–2), p 21–27.
15. H.S. Lee, J.K. Singh and J.H. Park, Pore Blocking Characteristics of Corrosion Products Formed on Aluminum Coating Produced by Arc Thermal Metal Spray Process in 3.5 wt.% NaCl Solution, *Constr. Build. Mater.*, 2016, **113**, p 905–916.
16. L.M. Liu, Z. Wang and G. Song, Study on Corrosion Resistance Properties of Hydrothermal Sealed Arc Sprayed Aluminium Coating, *Surf. Eng.*, 2010, **26**(6), p 399–406.
17. I.C. Park and S.J. Kim, Corrosion Behavior in Seawater of Arc Thermal Sprayed Inconel 625 Coatings with Sealing Treatment, *Surf. Coat. Tech.*, 2017, **325**, p 729–737.
18. S.J. de Mora, C. Stewart and D. Phillips, Sources and Rate of Degradation of Tri (n-butyl) Tin in Marine Sediments Near Auckland, New Zealand, *Mar. Pollut. Bull.*, 1995, **30**(1), p 50–57.
19. L.D. Chambers, C. Hellio, K.R. Stokes, S.P. Dennington, L.R. Goodes, R.J.K. Wood and F.C. Walsh, Investigation of Chondrus Crispus as a Potential Source of New Antifouling Agents, *Int. Biodeter. Biodegr.*, 2011, **65**(7), p 939–946.
20. S. Liu, X. Zhao, H.C. Zhao, H.Y. Sun and J.M. Chen, Corrosion Performance of Zinc Coated STEEL in Seawater Environment, *Chin. J. Oceanol. Limn.*, 2017, **35**(2), p 423–430.
21. J. Stoulil, B. Domko and J. Šerák, Corrosion Properties of Model Aluminium Alloys for Coating Steel Substrate, *Mater. Corros.*, 2017, **68**(1), p 77–81.
22. S.L. Zheng, C. Li, Q.T. Fu, W. Hu, T.F. Xiang, Q. Wang, M.P. Du, X.C. Liu and Z. Chen, Development of Stable Superhydrophobic Coatings on Aluminum Surface for Corrosion-Resistant, Self-Cleaning, and Anti-Icing Applications, *Mater. Design*, 2016, **93**, p 261–270.
23. J.D. Brassard, D.K. Sarkar, J. Perron, A. Audibert-Hayet and D. Melot, Nano-Micro Structured Superhydrophobic Zinc Coating on Steel for Prevention of Corrosion and Ice Adhesion, *J. Colloid Interf. Sci.*, 2015, **447**, p 240–247.
24. Y.C. Li, D.K. Xu, C.F. Chen, X.G. Li, R. Jia, D.W. Zhang, W.G. Sand, F.H. Wang and T.Y. Gu, Anaerobic Microbiologically

Influenced Corrosion Mechanisms Interpreted using Bioenergetics and Bioelectrochemistry: A Review, *J. Mater. Sci. Technol.*, 2018, **34**(10), p 1713–1718.
25. X.D. Zhao, K.F. Chen, J. Yang, G.F. Xi, H.T. Tian and Q.G. Chen, Effect of Chloride Ion Concentration on Corrosion of Q235 Steel in Sulfate-Reducing Bacteria Containing Solution, *Int. J. Electrochem. Sci.*, 2019, **14**, p 875–885.
26. W. Guo, J. Zhang, Y. Wu, S. Hong and Y. Qin, Fabrication and Characterization of Fe-Based Amorphous Coatings Prepared by High-Velocity Arc Spraying, *Mater. Design*, 2015, **78**, p 118–124.
27. H.S. Lee and J.K. Singh, Influence of Calcium Nitrate on Morphology and Corrosion Characteristics of Ammonium Phosphate Treated Aluminum Coating Deposited by Arc Thermal Spraying Process, *Corros. Sci.*, 2019, **146**, p 254–268.
28. X. Qiao, Y.M. Wang, W.X. Weng, B.L. Liu and Q. Li, Influence of Pores on Mechanical Properties of Plasma Sprayed Coatings: Case Study of YSZ Thermal Barrier Coatings, *Ceram. Int.*, 2018, **44**(17), p 21564–21577.
29. L. Qiao, Y.P. Wu, S. Hong and J. Cheng, Ultrasonic Cavitation Erosion Mechanism and Mathematical Model of HVOF Sprayed Fe-Based Amorphous/Nanocrystalline Coatings, *Ultrason. Sonochem.*, 2019, **52**, p 142–149.
30. S.U.N. Cheng and H.A.N. Enhou, Effects of Sulfate Reducing Bacteria on Corrosion of Zinc in Marine Sediment, *Chin. J. Nonferrous Met.*, 2003, **13**(5), p 1262–1266.
31. F. Liu, J. Zhang, S. Zhang, W. Li, J. Duan and B. Hou, Effect of Sulphate Reducing Bacteria on Corrosion of Al-Zn-In-Sn Sacrificial Anodes in Marine Sediment, *Mater. Corros.*, 2012, **63**(5), p 431–437.
32. Z.H. Wang, C.T. Chen, J.T. Jiu, S. Nagao, M. Nogi, H. Koga, H. Zhang, G. Zhang and K. Suganuma, Electrochemical Behavior of Zn-xSn High-Temperature Solder Alloys in 0.5 M NaCl Solution, *J. Alloy. Compd.*, 2017, **716**, p 231–239.
33. N. Barati, A. Yerokhin, F. Golestanifard, S. Rastegari and E.I. Meletis, Alumina-Zirconia Coatings Produced by Plasma Electrolytic Oxidation on Al Alloy for Corrosion Resistance Improvement, *J. Alloy. Compd.*, 2017, **724**, p 435–442.
34. Q.J. Zhu and K. Wang, Microstructure and Anti-corrosion Properties of Arc-Sprayed Aluminum Coating in Splash Zone, *Adv. Mater. Res. Trans Tech Publications Ltd*, 2011, **199**, p 1949–1953.
35. S.J. Kim, S.J. Lee, Y.S. Park, J.Y. Jeong and S.K. Jang, Influence of Sealing on Damage Development in Thermally Sprayed Al–Zn–Zr Coating, *Sci. Adv. Mater.*, 2014, **6**(9), p 2066–2070.
36. H.R. Jeong, H.S. Lee, P. Jalalzai, S.J. Kwon, J.K. Singh, R.R. Hussain, R. Alyousef, H. Alabduljabbar and F. Aslam, Sodium Phosphate Post-treatment on Al Coating: Morphological and Corrosion Study, *J. Therm. Spray Tech.*, 2019, **28**(7), p 1511–1531.
37. J.B. Cheng, X.B. Liang and B.S. Xu, Effects of Crystallization on the Corrosion Resistance of Arc-Sprayed FeBSiNb Coatings, *J. Therm. Spray Techn.*, 2014, **23**(3), p 373–379.
38. E.A. Esfahani, H. Salimijazi, M.A. Golozar, J. Mostaghimi and L. Pershin, Study of Corrosion Behavior of Arc Sprayed Aluminum Coating on Mild Steel, *J. Therm. Spray Tech.*, 2012, **21**(6), p 1195–1202.
39. P. Qi, D. Zhang and Y. Wan, Determination of Sulfate-Reducing Bacteria with Chemical Conversion from ZnO Nanorods Arrays to ZnS Arrays, *Sensor. Actuat. B- Chem.*, 2013, **181**, p 274–279.
40. Q. Jiang, Q. Miao, W.P. Liang, F. Ying, F. Tong, Y. Xu, B.L. Ren, Z.J. Yao and P.Z. Zhang, Corrosion Behavior of Arc Sprayed Al–Zn–Si–RE Coatings on Mild Steel in 3.5 wt% NaCl Solution, *Electrochim. Acta*, 2014, **115**, p 644–656.
41. L. Benea, A.C. Ciubotariu and W. Sand, Biofilm Formation and Corrosion Resistance of Ni/SiC Nanocomposite Layers, *Int. J. Mater. Res.*, 2013, **104**(5), p 489–497.
42. C. Xie, H. Li, X. Zhou and C. Sun, Corrosion Behavior of Cold Sprayed Pure Zinc Coating on Magnesium, *Surf. Coati. Tech.*, 2019, **374**, p 797–806.
43. B.J. Zheng, Y. Zhao, W.B. Xue and H.F. Liu, Microbial Influenced Corrosion Behavior of Micro-Arc Oxidation Coating on AA2024, *Surf. Coat. Tech.*, 2013, **216**, p 100–105.